Prediction of cooling-coil performance under condensing conditions

D. R. Mirth and S. Ramadhyani
Ray W. Herrick Laboratories, School of Mechanical Engineering, Purdue University, West Lafayette, IN, USA

The possibility of predicting chilled-water cooling-coil performance under condensing conditions using dry-surface heat transfer correlations is examined. Experimentally determined wet-surface Nusselt number data are presented and compared with dry-surface data obtained from the same cooling coils. The wet-surface Nusselt numbers show considerable scatter; some of the results are higher than the corresponding dry-surface correlations, while others are lower. A sensitivity analysis is presented to illustrate that the wet-surface Nusselt numbers are very sensitive to the uncertainties in the measured inlet dew-point temperature and the measured heat transfer rate. It is demonstrated that the use of dry-surface Nusselt number correlations in a coil model result in wet-surface heat transfer predictions that are generally within 5 percent of the experimentally determined value.

Keywords: cooling coil; fin tube heat exchanger; condensation

Introduction

Chilled-water cooling coils are plate-fin-tube heat exchangers that are used to cool and dehumidfy air in large building air conditioning systems. Figure 1 schematically depicts a typical four-row coil. The air enters the coil on the left side, as shown, and flows through passages formed by closely spaced wavy fin surfaces. Cold water flows in a cross-counterflow arrangement, cooling and dehumidifying the warm air.

When attempting to predict the heat transfer performance of such cooling coils, it is necessary to have an air-side heat transfer correlation that is valid for the specific coil geometry. The industry standard (ARI 1987) requires that two such correlations be developed for each coil geometry. One correlation is required for coils operating under dry-surface conditions, while another is to be used for coils operating under wet-surface conditions. As will shortly be discussed, several previous studies have indicated that the heat transfer coefficients under wet- and dry-surface conditions might be significantly different from each other. These studies differ on whether wet-surface heat transfer coefficients exceed, or are lower than, the dry-surface values.

In general, both the wet- and dry-surface heat transfer correlations are developed from laboratory tests, in which the coil heat transfer rates and the inlet and outlet dry-bulb and dew-point temperatures are measured over a range of operating conditions. The measurements are used as inputs to a coil heat transfer model to extract the unknown air-side heat transfer coefficients. It will be shown in this study that wet-surface heat transfer coefficients determined in this way are extremely sensitive to errors inherent in the measurements of dew-point temperature and overall heat transfer rate. Consequently, large uncertainties are associated with wet-surface heat transfer correlations. Conversely, however, when coil heat transfer models are used to predict coil performance, the predicted heat transfer rate is found to be relatively insensitive to variations in the air-side heat transfer correlations. In this paper, it will be shown that it is possible to predict heat transfer rates under a wide range of wet-surface conditions with good accuracy using only dry-surface heat transfer correlations. The results that will be presented are for coils operating with relatively low, inlet water temperatures (3–5°C), which are typical of air-conditioning systems employing thermal storage units

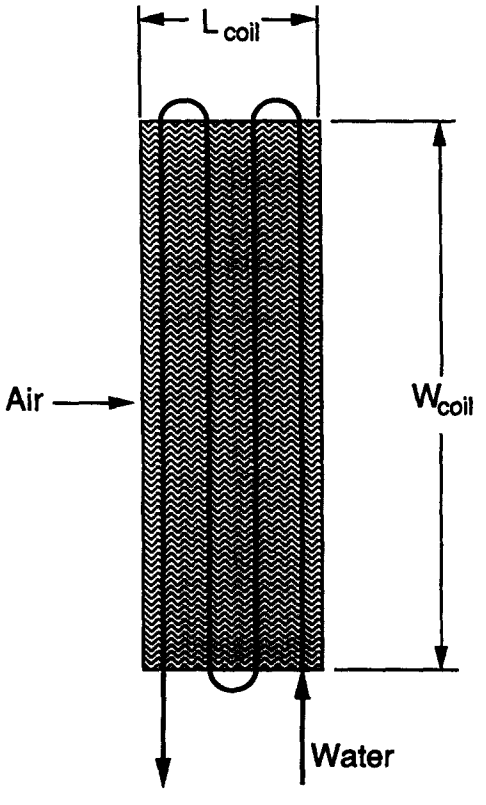

Figure 1 Schematic of a four-row chilled-water cooling coil

Address reprint requests to Professor Mirth at the Owens/Corning Technical Center 73-7, 2790 Columbus Road, Rt. 16, Granville, OH, USA.

Received 24 August 1992; accepted 17 February, 1993

(Nasr 1990). Because the condensation rate is greater at these relatively low water temperatures, an accurate prediction of the latent heat transfer due to condensation is especially important.

In the ensuing paragraphs, a brief review of previous papers reporting wet-surface heat transfer results will first be given. The experimental apparatus used to obtain the data presented in this paper, and the air-side heat transfer model used in the analysis, will then be described. This will be followed by a presentation and comparison of dry- and wet-surface Nusselt number data, along with a discussion of the sensitivity of these data to various experimental measurements. Finally, the validity and accuracy of using dry-surface Nusselt number correlations to predict wet-surface heat transfer performance will be addressed.

Literature review

When a surface is wetted, the water may interact with the airstream and change the heat transfer characteristics of the surface. Although results reported in the literature generally indicate that the sensible heat transfer coefficient increases when a surface is wetted, some authors have reported the opposite trend.

Bettanini (1970) found that the heat transfer coefficients for a wet surface were 10 percent higher than the dry-surface values for filmwise condensation and 35 percent higher for dropwise condensation on a vertical wall (with no tubes). In order to determine the reason for the increase in the heat transfer coefficient, Bettanini performed some dry-surface experiments with gypsum drops on the surface of the wall. He concluded that the flow disturbances caused by the drops enhanced the heat transfer, but not by the amount seen in the dropwise condensation experiments.

For developing flow between parallel plates (no tubes), Guillory and McQuiston (1973) reported heat transfer coefficients obtained under wet-surface conditions to be 30 percent higher than the corresponding dry-surface values. Tree and Helmer (1976) found that values of the heat transfer coefficient were the same under both dry- and wet-surface conditions for laminar flow between parallel plates with a fully developed velocity profile. This result is not surprising, since fully developed laminar flow is insensitive to roughness effects.

Jacobi and Goldschmidt (1990) studied the wet- and dry-surface behavior of a baffled, annular-finned-tube heat exchanger. The correlated wet-surface heat transfer coefficients were 17–50 percent lower than the correlated dry-surface values, with the largest discrepancy being at the lower Reynolds numbers. The authors speculated that the wet-surface heat transfer coefficients were lower due to flow blockage caused by condensate retention between adjacent fins.

For flat, plate-finned-tube heat exchangers, Myers (1967), Elmahdy (1975), and Eckels and Rabas (1987) reported 10–25 percent increases in the heat transfer coefficient under wet-surface conditions. McQuiston (1978a, 1987b), however, found that wet-surface conditions increased the heat transfer coefficient for flat plate coils with fewer than 10 fins per inch, and decreased it for coils with more than 10 fins per inch.

Notation

A_f	Surface area of fin
A_p	Surface area of primary surface
A_{step}	Total air-side surface area for a single step
A_{tot}	Total air-side surface area
C_{ari}	Parameter defined in Equation 18
c_p	Specific heat
CPO	Coil performance overprediction as defined in Equation 22
D_i	Tube inside diameter
D_o	Tube outside diameter
f	Friction factor
h	Heat transfer coefficient
h_{eff}	Effective heat transfer coefficient
i	Enthalpy
i_s	Equivalent saturated enthalpy
k	Thermal conductivity
L_t	Total tube length
L_{eq}	Length of equivalent efficiency straight fin
m	Fin efficiency parameter defined in Equation 4
$\dot{m}_{da}$	Mass flow rate of dry air
m''	The slope of the enthalpy-saturation temperature curve at the mean surface temperature
$\dot{m}_a$	Average air mass flow rate
$\dot{m}_w$	Water mass flow rate
N_{step}	Number of steps
Nu	Nusselt number
Pr	Prandtl number
q	Heat transfer rate
Q	Heat transfer rate
q_{step}	Heat transfer rate for individual step
R_{col}	Radius of fin collar
R_{eq}	Radius of equivalent area circular fin
R_f	Fin metal resistance
R_i	Water-side resistance
R_m	Total metal resistance
R_t	Tube wall resistance
R_{tot}	Total air-side resistance
Re	Reynolds number
s	Spacing between fins
T	Temperature
V_{max}	Maximum velocity
W	Parameter defined in Equation 10

Greek symbols

ΔP	Pressure drop
δ	Fin thickness
Φ	Fin efficiency
ν	Kinematic viscosity
η	Combined fin and prime surface efficiency
μ	Viscosity

Subscripts

a	Air
da	Dry air
dew	Dew point
dry	Dry surface condition
f	Fin
i	Inlet condition
ma	Moist air
o	Outlet condition
t	Tube
s	Equivalent saturated surface condition
w	Water
wet	Wet surface condition

For configured surfaces, such as corrugated or wavy fins, it might be expected that any heat transfer enhancement due to water on the surface would be reduced, since the fins already have mechanisms to disrupt and mix the flow. The available experimental evidence, however, is inconclusive. Senshu et al. (1981) noted no increase in the heat transfer coefficient for louvered fins, but Yoshii et al. (1983) reported a 20–40 percent increase in the heat transfer coefficient for a wavy, plate-finned cooling coil operating under wet-surface conditions. It thus appears that additional experimental data are required before this issue can be clarified.

Experimental apparatus

The purpose of the experimental setup was to obtain heat transfer and pressure drop data from commercially available chilled water cooling coils for a wide range of operating conditions. A summary of the geometric characteristics of the five coils tested is given in Table 1. Figure 2 provides a schematic representation of the fin-and-tube geometries of the cooling coils. The range of inlet air and water temperatures for each data run is listed in Table 2. The design of the experimental apparatus follows the general guidelines presented in ASHRAE Standard 33-78 (1978) and is briefly described in the following paragraphs.

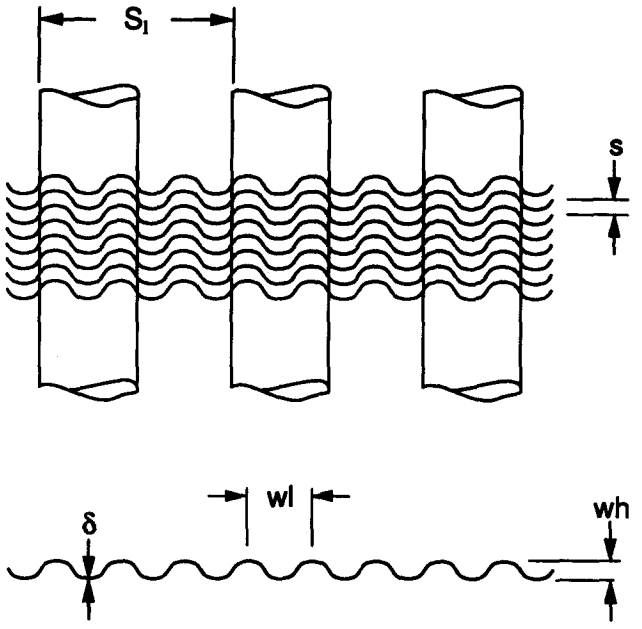

Figure 2 Schematic of the fin-and-tube geometries of the cooling coils

Table 1 Cooling coil geometries

	Coil 1	Coil 2	Coil 3	Coil 4	Coil 5
Manufacturer	A	A	A	B	B
Rows	8	8	4	4	8
s (mm)	3.05	1.47	1.47	2.11	2.11
D_o (mm)	13.2	13.2	13.2	16.4	16.4
D_i (mm)	12.4	12.4	12.4	15.3	15.3
S_t (mm)	31.8	31.8	31.8	38.1	38.1
Coil face height (m)	0.45	0.45	0.45	0.46	0.46
W_{coil} (m)	0.91	0.91	0.91	0.86	0.86
L_{coil} (m)	0.22	0.22	0.11	0.13	0.26
Circuiting	1	1	1	1/2	1/2
δ (mm)	0.15	0.15	0.15	0.15	0.15
wl (mm)	10.9	10.9	10.9	11.0	11.0
wh (mm)	2.38	2.38	2.38	3.25	3.25

Table 2 Range of inlet air and water conditions for wet-surface data

Coil	Run	$T_{dew,\,ai}$ (°C)	T_{ai} (°C)	T_{wi} (°C)	Face velocity (m/s)	Water velocity (m/s)
1	1	12.1–13.1	23.1–23.7	4.0–4.5	1.3–2.1	1.0
	2	12.0–12.2	26.2–26.9	4.2–4.4	1.3–2.1	1.0
	3	14.8–16.7	26.0–26.8	5.0–5.4	1.4–2.1	1.0
	4	15.0–16.5	23.3–25.3	4.6–4.7	1.2–2.1	0.80
	5	17.7–20.8	26.0–27.1	4.2–4.5	1.3–2.1	1.0
	6	19.5–20.5	24.9–25.6	4.5–5.0	1.3–2.1	1.0
2	1	18.8–19.7	28.5–30.2	5.1–6.3	1.1–1.8	1.0
	2	15.1–15.8	23.7–25.2	5.0–5.2	1.1–1.8	1.0
3	1	19.3–19.9	25.6–26.2	3.9–4.5	1.0–2.1	0.95
	2	15.1–18.5	22.5–23.0	3.1–3.4	1.1–2.2	0.93
4	1	12.2–12.5	24.7–25.0	3.2–3.3	1.3–2.9	1.1
	2	15.5–15.9	25.5–26.2	3.0–3.3	1.4–2.2	1.2
	2a	15.8–15.9	23.0–23.2	3.0–3.1	2.4–2.8	1.1
	3	19.7–20.2	24.9–25.1	3.3–3.5	1.3–2.2	1.2
	3a	18.6–19.0	23.9–24.0	3.3–3.5	2.4–2.7	1.1
5	1	12.2–12.7	23.6–24.5	3.1–3.2	1.3–2.3	1.1
	2	14.9–15.4	22.5–23.5	3.1–3.3	1.3–2.3	1.1
	3	17.8–18.6	25.2–25.9	3.3–3.6	1.3–1.9	1.1

Air side

A schematic of the experimental apparatus is shown in Figure 3. Air flow in the open-loop wind tunnel was provided by a centrifugal fan controlled through the use of a variable speed drive on the fan motor. The flow rate was determined by measuring the pressure drop across two or three (depending upon the flow rate) 152.4-mm (6-in.) diameter, long-radius flow nozzles. The pressure drop was measured by a differential pressure transducer, which was periodically calibrated against a precision pressure gage. The discharge coefficients of the nozzles were determined to be approximately 1.0 (ASHRAE 1985). The calibrated pressure transducer was capable of measuring the pressure drop with an accuracy of ± 1.0 mm of water. The resulting accuracy of the mass-flow measurements was ± 0.03 kg/s when three nozzles were in use (flow rates greater than 1 kg/s), and ± 0.015 kg/s when two nozzles were in use. This accuracy results in uncertainties in the air mass flow rate and their air-side Reynolds number of ± 3 percent.

In order to reduce fan-generated turbulence that could affect the heat transfer performance of the test coils (Zozulya 1973), a matrix of approximately 27,000 milk straws, followed by a wire screen, was placed 0.9 m upstream of the cooling coil. The straws, which were packed wall-to-wall in the duct, were 14.6 mm long and 3.2 mm in diameter. The wire screen had a mesh of 1.18 by 1.18 wires per mm. Loehrke and Nagib (1972) reported that this combination of straws and a screen would reduce free-stream turbulence levels to an acceptable level of 1–2 percent (free-stream turbulence is expressed as a ratio of the rms velocity fluctuation to mean velocity). These flow conditioners also served to flatten the velocity profile of the air entering the test section.

In order to humidify the air for the purpose of obtaining wet-surface data, a steam injector was placed in the duct immediately downstream of the fan. The steam flow rate was adjusted manually until the desired dew-point was reached at the inlet to the test section. Six meters (20 ft) of duct length was constructed between the steam injectors and the test section to ensure that the mist ejected from the steam line was completely evaporated before the air reached the cooling coil. O'Dell (1977) reported that 3–3.6 m (10–12 ft) of duct length was sufficient to completely evaporate the water droplets.

The dew-point was measured upstream and downstream of the coil using a chilled-mirror device at each location. The accuracy of the chilled-mirror devices was reported by the manufacturer to be ± 0.55°C. Before any wet-surface data were taken, the two chilled-mirror devices were compared with each other by placing them both in the duct and varying the dew-point temperature from 10°C to 20°C. The maximum difference between the measured dew-point temperatures was 0.34°C. The accuracy of the chilled-mirror devices was also checked by measuring the condensate runoff (through the use of a stopwatch and a graduated cylinder) from steady state, wet-surface tests, and comparing the results with those obtained using the measured inlet and outlet dew-point temperatures. The two different methods of determining the condensation rate initially produced results that were within 3 percent of one another. When this check was repeated after testing was completed on the first three coils, however, it was found that the different methods produced condensation rates that differed from each other by as much as 8.5 percent. The inlet and outlet chilled-mirror devices were subsequently compared with a new, more sophisticated chilled-mirror device that had a reported accuracy of ± 0.2°C. The new device

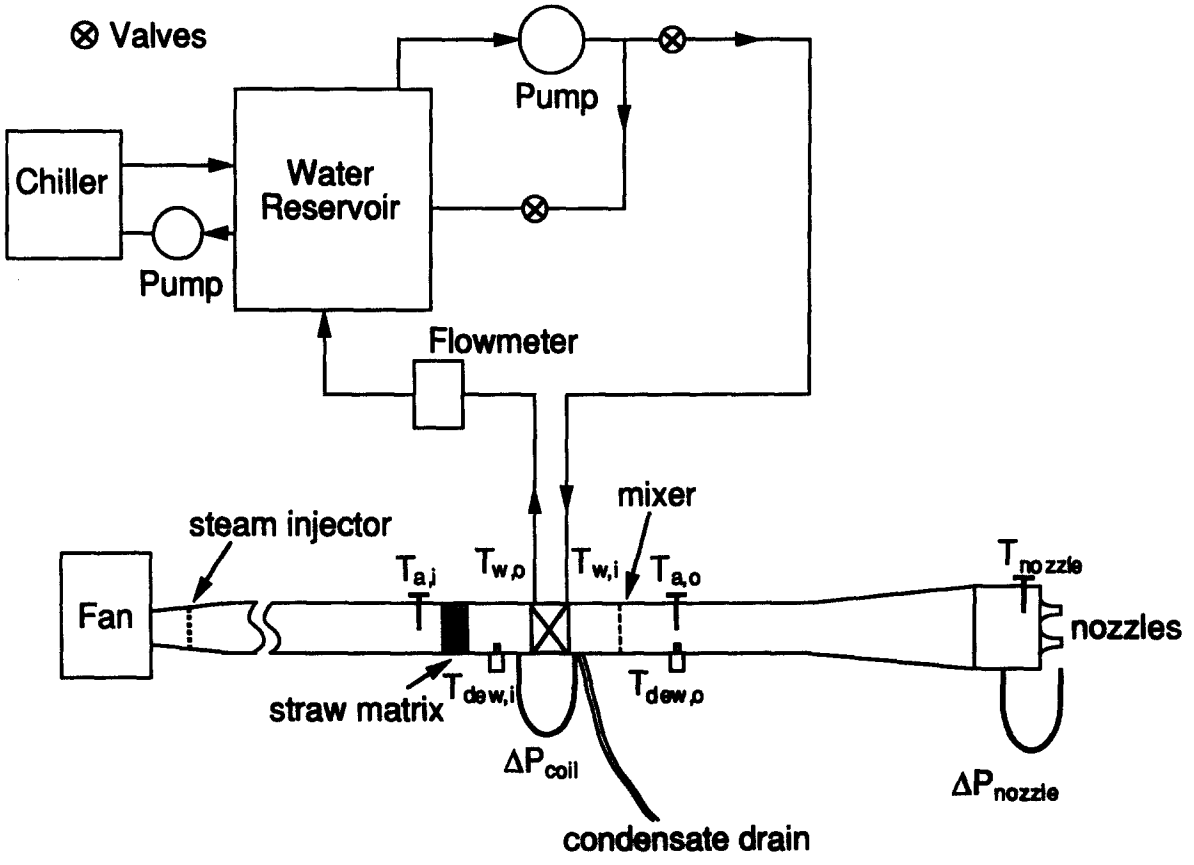

Figure 3 Schematic of the experimental apparatus

measured dew-point temperatures an average of 0.66°C higher than those measured by the chilled-mirror device installed at the inlet of the coil, while measuring an average of 0.4°C higher than the chilled-mirror device installed at the outlet of the coil. Consequently, the new device was used to measure the inlet dew-point temperatures for all subsequent tests (coils 4 and 5). The condensation rates for coils 4 and 5 were determined by directly measuring the condensate runoff.

The experimental apparatus did not include a means of controlling the air-side coil inlet temperature, $T_{a,i}$. Instead, the inlet air temperature was determined by the room conditions. Although the room temperature varied from about 20°C (68°F) to 28°C (83°F) over the course of the experimental testing, it was usually constant within 1°C (1.8°F) during the individual experimental runs.

All of the air-side temperatures were measured with individual platinum resistance temperature devices (RTDs). A louvered mixer was placed after the test coil to insure that a uniform temperature profile was achieved before the outlet air conditions were measured. Both the inlet and outlet coil air-temperature profiles were periodically checked to ensure that the profiles were uniform in both the vertical and horizontal directions.

The RTDs used to measure the inlet and outlet air temperatures were placed so that they could not "see" the cooling coil, thus eliminating any possible measurement errors from radiative effects. The inlet RTD was placed upstream of the straw matrix, while the outlet RTD was placed downstream of the mixer. Heat losses from the duct and cooling coils were minimized by heavily insulating the duct and the test section with a combination of fiberglass mat and foam-rubber sheet insulation. The insulation thickness was calculated to limit the heat loss to less than 1 percent of the coil's heat transfer rate.

All of the RTDs used to measure the air and water temperatures were periodically checked by placing them in a water bath along with a mercury-in-glass thermometer that could be accurately read to within ± 0.1°C. The temperatures measured by the RTDs agreed within ± 0.16°C of those measured by the thermometer.

Water side

The water flow rate was controlled by manually adjusting one or more of the valves shown in Figure 3. The mass flow rate of the water was measured with a Coriolis mass flowmeter. The factory calibration of this flowmeter resulted in a reported accuracy of ± 0.5 percent for the mass flow rates used in this study (around 1 kg/s). This calibration was checked by comparing the mass flow rate measured by the flowmeter with the flow rate obtained using a weigh tank. The values determined using the weigh tank were within 1 percent (which is the approximate accuracy of the scale) of those obtained from the flowmeter.

The chiller was run continuously during each experiment. The water in the reservoir was maintained at a constant temperature by adding city water to the reservoir at a rate that balanced the chiller's load with its capacity. Thus, the city-water flow rate was adjusted until the inlet water temperature, $T_{w,i}$, was constant. In accordance with recommended practice (ASHRAE 1978), the RTDs used to measure the inlet and outlet water temperatures were placed immediately downstream of two consecutive 90° bends in order to ensure that the water was well mixed at the point of measurement.

The heat transfer rate of the coil was determined by averaging the values obtained independently from the air side and the water side of the cooling coil. For each side, the heat transfer rate was calculated by multiplying the fluid mass flow rate by the enthalpy change between inlet and outlet. The differences between the air-side and the water-side heat transfer rates were less than 5 percent for all the data reported in this paper, and less than 3 percent for 80 percent of the data.

Coil model

This section will describe the coil model that was used to reduce the experimental data, as well as to predict coil performance. The following basic assumptions were used in this model:

(1) the air-side heat transfer coefficient, h, was assumed to be constant through the coil;
(2) air and water properties were evaluated at the average of the inlet and outlet temperatures; and
(3) psychrometric relations were obtained from equations given in O'Dell (1977).

The air-side of the coil was modeled using essentially the same procedure as given in ARI Standard 410-87 (1987). The only noteworthy difference is that the present model uses a discretized approach, as opposed to ARI's log-mean-temperature-difference (or enthalpy-difference, for wet surfaces) approach. The coil is modeled as a pure counter-flow heat exchanger. Each tube is actually perpendicular to the air flow direction, but the several tube passes considered together result in a configuration that is effectively counterflow. The counterflow model for such coils has been shown to be valid if the number of tube passes exceeds three (Stevens 1957). The coil is discretized into 600 sections in the air flow direction, and calculations are conducted for each section by marching along the sections from air inlet to outlet. The number of discrete steps was selected after a numerical study indicated that the solution was insensitive to further increases in the number of steps. The accuracy was further verified by demonstrating that results obtained for a dry coil using this step size were well within 1 percent of results obtained using a log-mean-temperature-difference approach, all other variables being equal. The present approach offers the advantage of calculating the variations in fin efficiency along the length of the coil instead of utilizing a single constant value. In addition, this approach offers the flexibility of utilizing alternative procedures for calculating the air-side heat transfer that cannot be implemented via a log-mean-enthalpy-difference approach.

In order to use the program to predict the performance of a coil, an initial guess for the outlet water temperature is required. The program involves a step-by-step march through the coil in the direction of increasing x, as shown in Figure 4. The free-stream and coil surface conditions are calculated at each step (see Figure 4) using the appropriate dry- or wet-surface heat transfer equations. At the end of the heat exchanger, the program checks the calculated water inlet temperature with the given inlet temperature. If the two values differ by more than a prespecified tolerance, the program adjusts the value of the outlet water temperature and repeats the calculation. Iterations are continued until convergence is achieved.

As noted previously, the heat and mass transfer on the air side is modeled using the method outlined in ARI Standard 410-87. The definitions of certain basic parameters needed in the calculations will now be provided, along with a brief description of how each is determined.

For a dry coil, the fin efficiency, Φ, is found using the method presented by Schmidt (1949) for an annular fin that has an area equivalent to the hexagonal unit cell around each tube in an equilateral triangle arrangement. For a wet fin, the same procedure is followed, except that an effective heat transfer

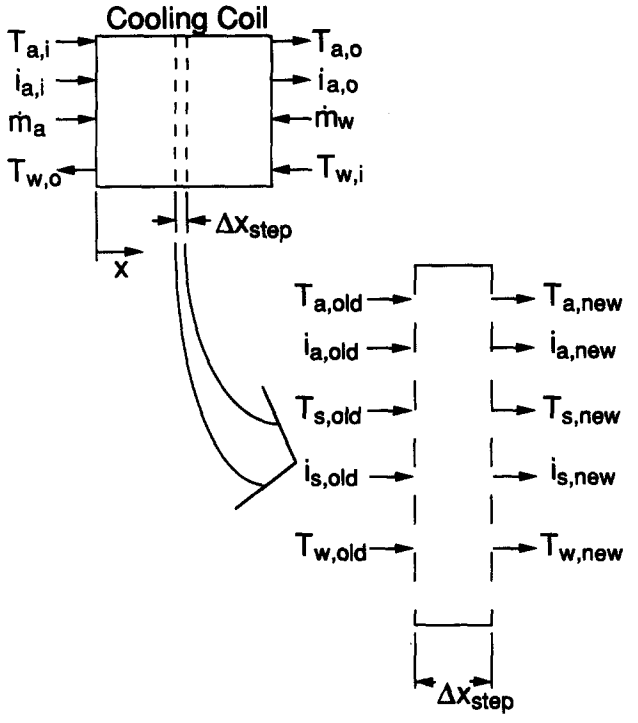

Figure 4 Schematic of coil model discretization

coefficient is used in the fin-efficiency calculation

$$h_{eff} = h_{dry} \quad \text{(dry fin)} \tag{1}$$

$$h_{eff} = \frac{h_{wet} m''}{c_{p,\,ma}} \quad \text{(wet fin)} \tag{2}$$

m'', which is depicted schematically in Figure 5, is the slope of the enthalpy-saturation temperature curve for moist air at the mean surface temperature, T_s. The efficiency is then found from

$$\Phi = \frac{\tanh(mL_{eq})}{mL_{eq}} \tag{3}$$

where

$$m = \left(\frac{2h_{eff}}{k_f \delta}\right)^{0.5} \tag{4}$$

and

$$L_{eq} = (R_{eq} - R_{col})\left[1 + 0.35 \ln\left(\frac{R_{eq}}{R_{col}}\right)\right] \tag{5}$$

Equation 3 is the analytical expression for the efficiency of a straight fin. L_{eq} is defined in such a way as to permit the use of this equation to calculate the efficiency of an annular fin (Schmidt 1949).

The efficiency of the total surface (including the fin and the prime surface) is found from

$$\eta = \frac{\Phi A_f + A_p}{A_{tot}} \tag{6}$$

The fin metal resistance for a wet surface, R_f, is given by

$$R_f = \left(\frac{1-\eta}{\eta}\right)\left(\frac{1}{h_{eff} A_{tot}}\right) \tag{7}$$

The total mean resistance, R_m, is the summation of the tube wall resistance, R_t, and R_f,

$$R_m = R_t + R_f \tag{8}$$

where

$$R_t = \frac{\ln\left(\frac{D_o}{D_i}\right)}{2\pi k_t L_t} \tag{9}$$

The sequence of calculations performed at each step will now be described. When a forward step is taken, the surface is initially assumed to be wet. In accordance with the procedure given in ARI (1987), the equivalent saturated surface temperature, T_s, and the corresponding saturated enthalpy, i_s, are first calculated at that location in the heat exchanger, using a resistance network between the water and the free-stream air conditions. This calculation involves defining the parameter

$$W \equiv \frac{R_m + R_i}{c_{p,\,ma}\left(\frac{1}{h_{wet} A_{tot}}\right)} \tag{10}$$

where

$$R_i = \frac{1}{h_i A_i} \tag{11}$$

The water-side heat transfer coefficient, h_i, is determined from the correlation developed by Gnielinski (1976):

$$\mathrm{Nu} = \frac{(f/8)(\mathrm{Re} - 1000)\mathrm{Pr}}{1 + 12.7(f/8)^{1/2}(\mathrm{Pr}^{(2/3)} - 1)} \tag{12}$$

where the friction factor, f, is given by

$$f = (0.79 \ln \mathrm{Re} - 1.64)^2 \tag{13}$$

T_s and i_s are related to W through the following equation:

$$W = \frac{T_{s,\,new} - T_{w,\,old}}{i_{a,\,old} - i_{s,\,new}} \tag{14}$$

The two unknowns, $T_{s,new}$ and $i_{s,new}$ in Equation 14, are calculated by solving the equation iteratively in conjunction with the psychometric relationship between T_s and i_s. If T_s is less than the free-stream dew-point temperature, the following wet-surface equations are used to find the desired parameters.

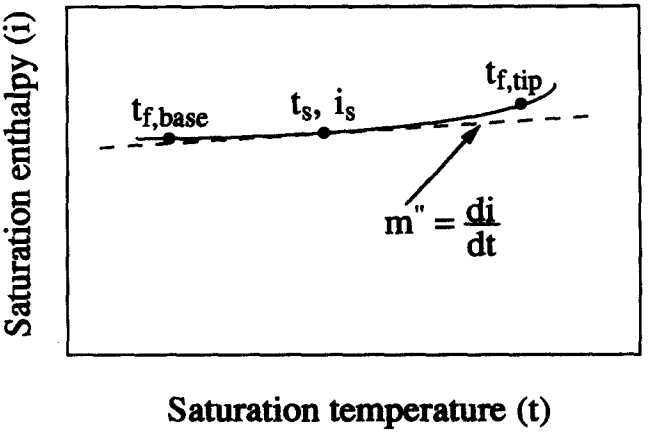

Figure 5 Schematic representation of the slope of the enthalpy saturation curve, m'', at the mean surface temperature, T_s

Otherwise, dry-surface equations, presented subsequently, are used.

For a wet surface, the heat transfer at each step is found from

$$q_{step} = \frac{h_{wet} A_{step}}{c_{p,\,ma}} (i_{a,\,old} - i_{s,\,new}) \tag{15}$$

An energy balance is then used to find the new value of free-stream enthalpy and the new water temperature as follows:

$$q_{step} = \dot{m}_a(i_{a,new} - i_{a,old}) = \dot{m}_w c_{p,w}(T_{w,new} - T_{w,old}) \tag{16}$$

The new dry-bulb temperature is found from

$$T_{a,new} = T_s + (T_{a,old} - T_s)\exp(-C_{ari}) \tag{17}$$

where

$$C_{ari} = \frac{A_{step} h_{wet}}{\dot{m}_{da} c_{p,\,ma}} \tag{18}$$

A_{step} is the air-side surface area for an individual step. If T_s is determined to be greater than the dew-point temperature, the dry-surface equations must be used. To this end, the heat transfer at each step is found from

$$q_{step} = \frac{1}{N_{step}} \left(\frac{T_{a,\,old} - T_{w,\,old}}{R_i + R_a + R_t} \right) \tag{19}$$

where

$$R_a = \frac{1}{\eta h_{dry} A_{tot}} \tag{20}$$

The new air and water temperatures are then calculated using an energy balance

$$q_{step} = \dot{m}_a c_{p,ma}(T_{a,new} - T_{a,old}) = \dot{m}_w c_{p,w}(T_{w,new} - T_{w,old}) \tag{21}$$

Once the new air and water conditions have been determined, another step is taken in the direction of the air flow, and the process is repeated.

Results

Comparison of dry- and wet-surface Nusselt number data

Dry-surface Nusselt number correlations were obtained from experimental data for each of the five coils tested in this study, and are listed in Table 3. Figures 6 and 7 show two of these correlations plotted with the dry-surface data for coils 1 and 4. The air-side Nusselt number, plotted on the ordinate, is defined as

$$\mathrm{Nu}_a = \frac{h(2s)}{k_a} \tag{22}$$

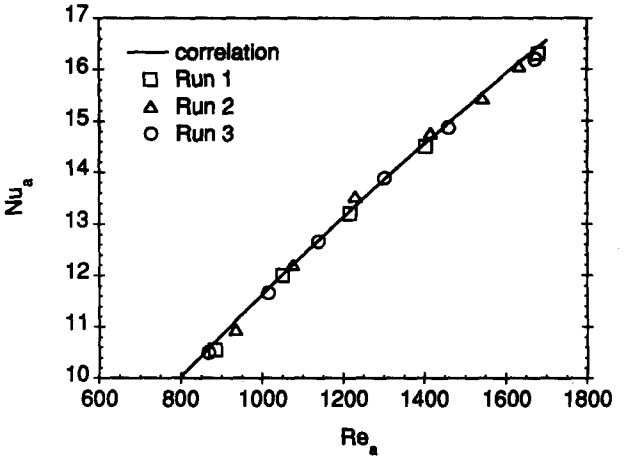

Figure 6 Dry-surface data plotted with the dry-surface correlation for coil 1

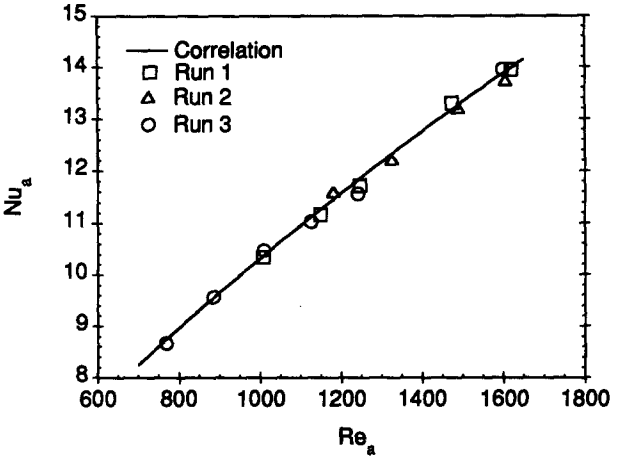

Figure 7 Dry-surface data plotted with the dry-surface correlation for coil 4

The air-side Reynolds number is defined as

$$\mathrm{Re}_a = \frac{V_{max}(2s)}{\nu_a} \tag{23}$$

where V_{max} is the air velocity calculated at the minimum cross-sectional area on the air side of the coil. Both figures illustrate the excellent repeatability in the determination of the dry-surface heat transfer coefficients. As shown in Table 3, the standard deviation of the data from the dry-surface correlations is less than 0.17 for all five coils.

Table 3 Dry-surface Nusselt number correlations

Coil	Dry-surface correlation	Range of data	Standard Deviation
1	$\mathrm{Nu}_a = 0.130\ \mathrm{Re}_a^{0.67}\mathrm{Pr}_a^{1/3}$	$473 < \mathrm{Re}_a < 785$	0.095
2	$\mathrm{Nu}_a = 0.011\ \mathrm{Re}_a^{0.98}\mathrm{Pr}_a^{1/3}$	$867 < \mathrm{Re}_a < 1680$	0.115
3	$\mathrm{Nu}_a = 0.327\ \mathrm{Re}_a^{0.60}\mathrm{Pr}_a^{1/3}$	$441 < \mathrm{Re}_a < 878$	0.147
4	$\mathrm{Nu}_a = 0.149\ \mathrm{Re}_a^{0.63}\mathrm{Pr}_a^{1/3}$	$1007 < \mathrm{Re}_a < 1598$	0.114
5	$\mathrm{Nu}_a = 0.0545\ \mathrm{Re}_a^{0.75}\mathrm{Pr}_a^{1/3}$	$712 < \mathrm{Re}_a < 1440$	0.167

Figures 8, 9, and 10 show dry-surface correlations plotted along with wet-surface Nusselt numbers for coils 1, 3, and 4, respectively. The different wet-surface data runs are distinguished primarily by differences in the inlet dew-point temperature. In marked contrast to the dry-surface data, Figure 11 illustrates the large amount of data scatter that is possible when attempting to determine wet-surface heat transfer coefficients. The wet-surface results scatter around the dry-surface correlation, with the average value being slightly higher than the corresponding dry-surface result. In general, the wet-surface Nusselt numbers for this coil decrease with increasing inlet dew-point temperature. The wet-surface data for coil 3 shown in Figure 9, on the other hand, are in good agreement with the dry-surface correlation for both data runs. The wet-surface Nusselt number data for coil 4, shown in Figure 10, lie uniformly below the dry-surface values and display considerable scatter. Variations of the wet-surface data with the inlet dew-point are not systematic for this coil. A comparison of the data for these three coils thus indicates that the wet-surface Nusselt numbers display much greater scatter than the dry-surface values and inconclusive trends with respect to variations in the inlet dew-point temperatures.

In order to provide perspective on the cause of this scatter in the wet-surface data, a sensitivity analysis of the data was undertaken. The uncertainties associated with the experimental

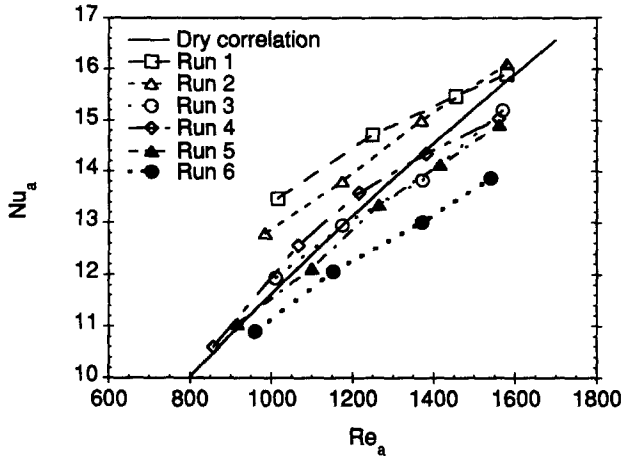

Figure 8 Wet-surface data plotted with the dry-surface correlation for coil 1

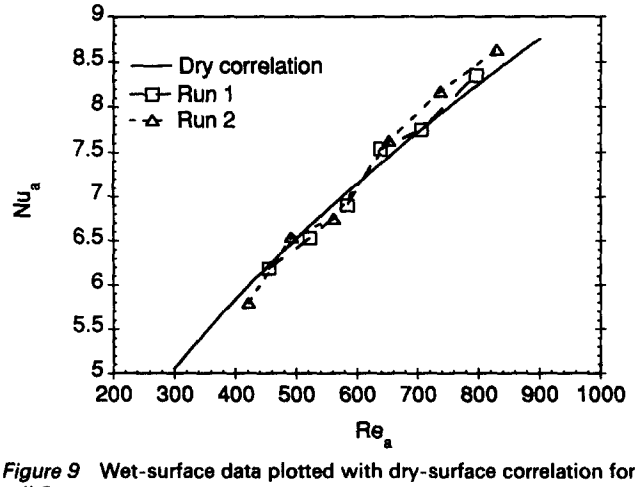

Figure 9 Wet-surface data plotted with dry-surface correlation for coil 3

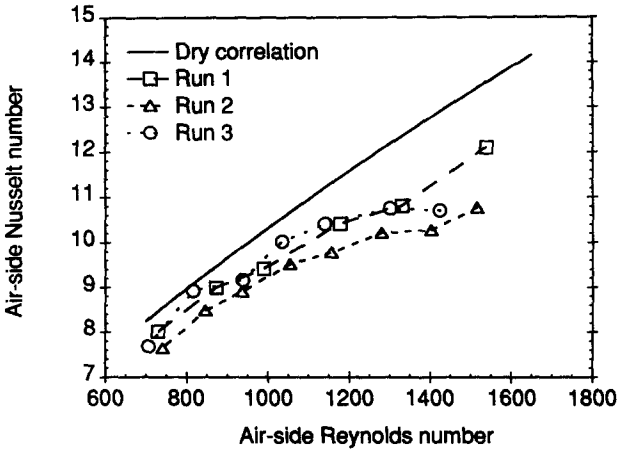

Figure 10 Wet-surface data plotted with the dry-surface correlation for coil 4

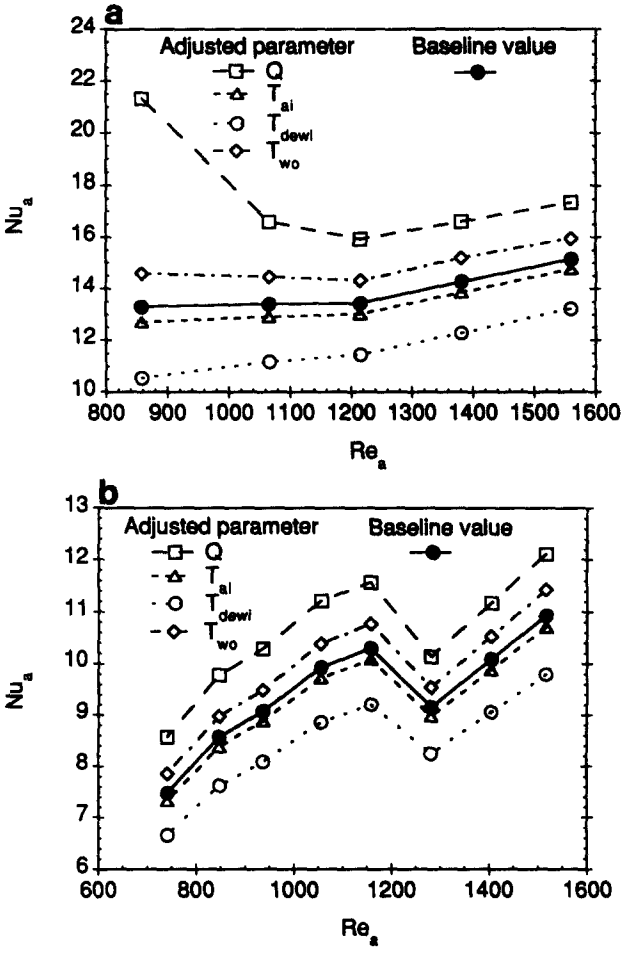

Figure 11 Sensitivity of the reduced wet-surface, air-side Nusselt numbers to increases in the measured heat transfer rate, and inlet air, water and dew-point temperatures: (a) coil 1, run 4; (b) coil 4, run 2

measurements of the inlet air, water and dew-point temperatures, and the heat transfer rate were first estimated. The estimated maximum measurement error for these parameters are

Air and water temperatures ± 0.2°C
Dew-point temperature ± 0.6°C
Heat transfer rate ± 3 percent

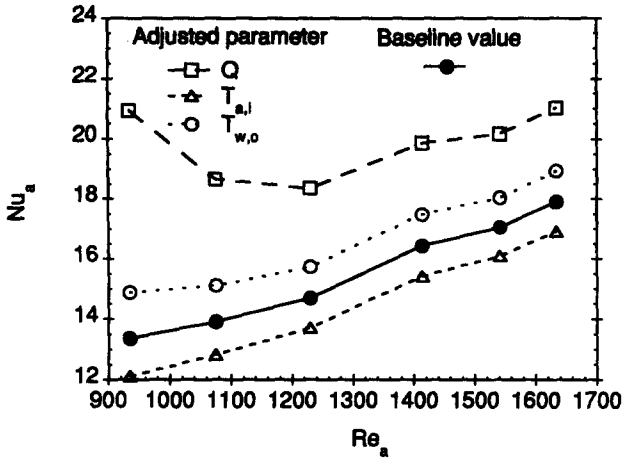

Figure 12 Sensitivity of the reduced dry-surface, air-side Nusselt numbers to increases in the measured heat transfer rate, and inlet air and water temperatures (coil 1, run 3)

Nusselt numbers were then predicted by increasing each of the parameters in turn, from their baseline values, by the extent of the estimated uncertainty. To simplify the sensitivity analysis, the average heat transfer rate was assumed to be constant (except, of course, when studying the sensitivity to variations in the measured heat transfer rate) and equal to the originally determined water-side heat transfer rate. Figures 11a and 11b illustrate the effect of these variations on experimentally determined wet-surface Nusselt numbers from coils 1 and 4, while Figure 12 shows their effect on dry-surface data from coil 1.

These figures show that the computed Nusselt number is extremely sensitive to small changes in the measured heat transfer rate. As can be seen in Figures 11a and 12, this sensitivity can be especially severe at low air-side Reynolds numbers (thus low air-side mass flow rates). This sensitivity is due to the fact that, when the heat transfer coefficient is increased in the data-reduction program in order to match the increase in the given heat transfer rate, the temperature difference between the air and the finned-tubes, which drives the heat transfer, is decreased. The decreased temperature difference necessitates a further increase in the heat transfer coefficient. Thus, the required proportion of change in the heat transfer coefficient exceeds the change in the heat transfer rate. The sensitivity is more severe at low air-side flow rates because the coil is asymptotically approaching its maximum possible heat transfer rate for the given water-side conditions (achieved when the air temperature is equal to temperature of the tube surface at the outlet of the coil), and further increases in the air-side heat transfer coefficient have a diminishing impact on the predicted heat transfer rate.

Varying the inlet dew-point temperature by the maximum estimated error in its measurement also results in large differences in the computed Nusselt numbers. The Nusselt number is sensitive to the inlet dew-point temperature, since the dew-point controls the driving force for latent heat transfer, which can be half or more of the total heat transfer of the coil. When the dew-point temperature is increased, the data-reduction program reduces the heat transfer coefficient in order to maintain the same total heat transfer rate. As the heat transfer coefficient is decreased, however, the temperature of the coil surface also decreases, thus increasing the driving force values for sensible and latent heat transfer. These increases in the driving forces cause the need for a further reduction in the heat transfer coefficient, thus causing the Nusselt number to be highly sensitive to small changes in the dew-point temperature.

The air-side Nusselt number is also sensitive to small changes in the inlet air and water temperatures, but the relatively small estimated errors associated with measuring these temperatures cause these measurements to be less serious sources of uncertainty in the reduced Nusselt number values.

It is believed that the scatter and nonrepeatability of the wet-surface Nusselt number data are primarily due to the uncertainty and nonrepeatability of the dew-point temperature measurements, and the related task of determining the air-side latent heat transfer rate. Although the dry- surface Nusselt number is very sensitive to errors in the experimentally determined heat transfer rate, the determination of this heat transfer rate is considerably more accurate and repeatable when there is no latent heat transfer occurring on the air side of the coil.

Use of dry-surface correlation to predict wet-surface heat transfer

While the studies listed previously compared wet- and dry-surface heat transfer coefficients, the more important consideration is whether or not a model using a dry-surface Nusselt number correlation can predict the wet-surface heat transfer performance. In order to address this issue, the dry-surface heat transfer correlations developed for each of the five coils used in this study were inserted into the coil model, which was then used to predict wet-surface performance. The results are presented in terms of a percent overprediction (CPO), which is defined as

$$\mathrm{CPO} = \left(\frac{Q_{\text{predicted}} - Q_{\text{experimental}}}{Q_{\text{experimental}}} \right) \times 100 \qquad (24)$$

The model was used to predict the wet-surface heat transfer rates for over 80 data points taken from tests on the five coils. The results of these predictions are shown in Figure 13. It can be seen that, with the exception of two points, the model using dry-surface correlations was able to predict the heat transfer rate within ± 5 percent of the experimentally measured value. The results shown in Figure 13 demonstrate that, despite the fact that the impact of condensation on the heat transfer coefficient is as yet unresolved, it is still possible to accurately predict wet-surface heat transfer performance using dry-surface heat transfer correlations.

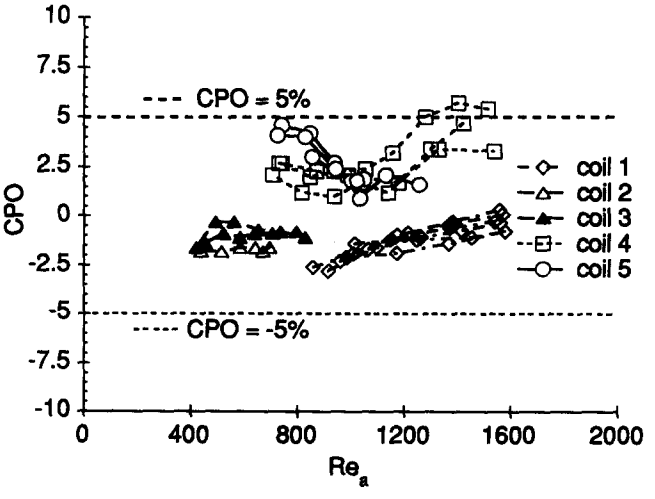

Figure 13 Coil performance predictions under condensing conditions using dry-surface correlations to determine the air-side heat transfer coefficient

Summary

Experimentally determined wet-surface Nusselt number data were presented and compared with dry-surface data obtained from the same cooling coils. The wet-surface Nusselt numbers showed considerable scatter, with some of the wet-surface results being higher than the corresponding dry-surface correlations, while others were lower than the dry-surface values. A sensitivity analysis revealed that the wet-surface Nusselt numbers were very sensitive to the uncertainties in the measured inlet dew-point temperature and the measured heat transfer rate. It was also determined that the use of dry-surface Nusselt number correlations in a coil model resulted in wet-surface heat transfer predictions that were generally within 5 percent of the experimentally determined value.

Acknowledgments

This research was conducted under EPRI contract RP2732-11. The program manager for this project was Mukesh Khattar.

References

ARI. 1987. ARI Standard 410-87: Forced-circulation air-cooling and air-heating coils. Air-Conditioning and Refrigeration Institute, Arlington, VA

ASHRAE. 1985. *ASHRAE Handbook: 1985 Fundamentals.* American Society of Heating, Refrigerating, and Air-Conditioning Engineers, Atlanta, GA

ASHRAE. 1978. ASHRAE Standard 33-78: Methods of testing forced circulation air cooling and air heating coils. American Society of Heating, Refrigerating, and Air-Conditioning Engineers, Atlanta, GA

Bettanini, E. 1970. Simultaneous heat and mass transfer on a vertical surface. *Int. Inst. Refrigeration Bull.*, **70**(1), 309–317

Eckels, P. W. and Rabas, T. J. 1987. Dehumidification: On the correlation of wet and dry transport processes in plate finned-tube heat exchangers. *J. Heat Transfer*, **109**, 575–582

Elmahdy, A. H. 1975. *Analytical and Experimental Multi-Row, Finned-Tube Heat Exchanger Performance during Cooling and Dehumidification Processes.* Ph.D. Thesis, Mechanical Engineering Dept., Carleton University, Ottawa, Canada

Gnielinski, V. 1976. New equations for heat and mass transfer in turbulent pipe and channel flow. *Int. Chem. Eng.*, **16**, 359–368

Guillory, J. and McQuiston, F. 1973. An experimental investigation of air dehumidification in a parallel plate. *ASHRAE Trans.*, **79**(2), 146–151

Jacobi, A. M. and Goldschmidt, V. W. 1990. Low Reynolds number heat and mass transfer measurements of an overall counterflow, baffled, finned-tube, condensing heat exchanger. *Int. J. Heat Mass Transfer*, **33**(4), 755–765

Loehrke, R. I. and Nagib, H. M. 1972. Experiments on management of free-stream turbulence. AGARD Report No. 598, NATO

McQuiston, F. C. 1978a. Heat, mass and momentum transfer data for five plate-fin-tube heat transfer surfaces. *ASHRAE Trans.*, **84**(1), 266–293

McQuiston, F. C. 1978b. Correlation of heat, mass and momentum transport coefficients for plate-fin-tube heat transfer surfaces with staggered tubes. *ASHRAE Trans.*, **84**(1), 294–308

Myers, R. J. 1967. *The Effect of Dehumidification on the Air-Side Heat Transfer Coefficient for a Finned-Tube Coil.* M.S. thesis, Mechanical Engineering Dept., University of Minnesota, Minneapolis, MN

Nasr, K. 1990. *Energy Use Estimates of Ice Storage/Heat Recovery Systems in Large Office Buildings.* M.S. thesis, Mechanical Engineering Dept., Purdue University, West Lafayette, IN

O'Dell, L. 1977. Considerations for sizing and installing commercial and industrial steam humidifiers. *ASHRAE Trans.*, **83**, 745–750

Schmidt, E. 1949. Heat transfer calculation for extended surfaces. *J. ASRE*, **57**, 351–357

Senshu, T., Hatada, T., and Ishibane, K. 1981. Heat and mass transfer performance of air coolers under wet conditions. *ASHRAE Trans.*, **87**, 109–115.

Stevens, R. A., Fernandez, J., and Woolf, J. 1957. Mean temperature difference in one- two- and three-pass crossflow heat exchangers. *Trans. ASME*, **79**, 287–297

Tree, D. and Helmer, W. 1976. Experimental heat and mass transfer data for condensing flow in a parallel plate heat exchanger. *ASHRAE Trans.*, **82**, 289–299

Yoshii, T., Yamamoto, M., and Otaki, T. 1973. Effects of dropwise condensate on wet surface heat transfer of air cooling coils. *Proc. 13th Int. Congress of Refrigeration*, 285–292

Zozulya, N. V., Vorob'yeu, Yu. P., and Khauin, A. A. 1973. Effect of flow turbulization on heat transfer in a finned-tube bundle. *Heat Transfer Soviet Res.*, **5**(1), 154–156